

---

# PriorCVAE: Scalable MCMC Parameter Inference with Bayesian Deep Generative Modelling

---

Elizaveta Semenova  
University of Oxford

Prakhar Verma<sup>1</sup>  
Aalto University

Max Cairney-Leeming<sup>2</sup>  
ISTA (Institute of Science  
and Technology Austria)

Arno Solin  
Aalto University

Samir Bhatt  
University of Copenhagen  
Imperial College London

Seth Flaxman  
University of Oxford

## Abstract

Recent advances have shown that GP priors, or their finite realisations, can be encoded using deep generative models such as variational autoencoders (VAEs). These learned generators can serve as drop-in replacements for the original priors during MCMC inference. While this approach enables efficient inference, it loses information about the hyperparameters of the original models, and consequently makes inference over hyperparameters impossible and the learned priors indistinct. To overcome this limitation, we condition the VAE on stochastic process hyperparameters. This allows the joint encoding of hyperparameters with GP realizations and their subsequent estimation during inference. Further, we demonstrate that our proposed method, PriorCVAE, is agnostic to the nature of the models which it approximates, and can be used, for instance, to encode solutions of ODEs. It provides a practical tool for approximate inference and shows potential in real-life spatial and spatiotemporal applications.

## 1 INTRODUCTION

In numerous applied domains, Gaussian processes (GPs, Williams and Rasmussen, 2006) have emerged as the preferred priors within Bayesian hierarchical frame-

---

<sup>1</sup>This work was done when Prakhar Verma was visiting the University of Oxford. <sup>2</sup> This work was done when Max Cairney-Leeming was at the University of Oxford. For correspondence: elizaveta.p.semenova@gmail.com.

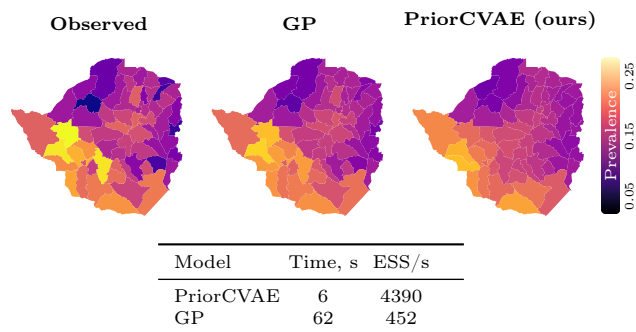


Figure 1: PriorCVAE versus GP inference on HIV Prevalence in Zimbabwe. PriorCVAE runs 10× faster than the GP model and gives competitive results.

works. Their wide adoption in environmental sciences (Dai et al., 2022), geosciences (Axen et al., 2022), agriculture (Belda et al., 2021), the pharmaceutical industry (Obrezanova et al., 2007; Schroeter et al., 2007; Semenova et al., 2021; Shapovalova et al., 2022), remote sensing (You et al., 2017), robotics (Deisenroth et al., 2013), and active learning (Krause and Guestrin, 2007) can be attributed to their versatility as universal approximators, depending on the covariance function, and their analytical convenience when used with a Gaussian likelihood. Despite these advantages, limitations arise when applying GPs to real-world tasks: inference scales cubically with the number of observed data points, making characterising uncertainty with *fully Bayesian* inference (incl. hyperparameters, see Fig. 1) prohibitively computationally expensive (see Doucet, 2010).

Deep generative models offer a pathway to address the scaling challenge of GPs in fully Bayesian modelling. GP priors and a wider range of stochastic processes can be encoded using variational autoencoders (VAEs, Kingma and Welling, 2013). Recently, a group of two-

stage methods has been proposed in the literature:  $\pi$ VAE (Mishra et al., 2022) encoding stochastic processes, and PriorVAE (Semenova et al., 2022) encoding realisations thereof. By training a VAE on draws from a stochastic process prior and using the trained decoder as a surrogate for the original GP during Bayesian inference, PriorVAE effectively sidesteps the computational overhead associated with GPs. This enables fast and efficient inference using methods like Markov chain Monte Carlo (MCMC). However, there is a serious drawback in this approach: while  $\pi$ - and PriorVAE encode function values, neither can explicitly encode and estimate hyperparameters. In this work, we propose to overcome this issue with a conditional variational autoencoder (CVAE, Sohn et al., 2015) architecture.

This paper introduces the novel PriorCVAE approach, which employs the conditional VAE framework to shift learning emphasis towards priors, rather than solely on observed data. The major advantage is the ability to condition on the hyperparameters of the priors, which retains both the benefits of reduced computation times and high effective sample sizes as seen with PriorVAE, but also endows the model with a capacity for clear prior identification. Consequently, downstream MCMC tasks can now explicitly estimate hyperparameters. This integration is especially promising for spatial and spatiotemporal inference, as shown in the experiments, offering a robust class of approximate GP models, and our new method is versatile and seamlessly integrates with well-known probabilistic programming frameworks such as Stan (Carpenter et al., 2017), NumPyro (Phan et al., 2019), PyMC (Oriol et al., 2023), and others (Štrumbelj et al., 2023). Even though this work was originally motivated by the problem of GP scalability, the proposed method is agnostic to the model that it approximates. For example, solutions of dynamical systems described by ordinary differential equations can also be encoded as we show in one of the experiments.

Our contributions are summarised as follows:

- We propose the PriorCVAE method that can ‘identify’ the learned priors by introducing a conditional variational autoencoder architecture, allowing us to explicitly encode hyperparameters and estimate them at the inference stage;
- We show that PriorCVAE can extrapolate prior draws with respect to hyperparameters—*i.e.* we can draw priors for values of hyperparameters which the PriorCVAE was not trained on;
- We demonstrate for the first time the applicability of the method to GPs with non-stationary kernels, and show that properties of functions obtained via

non-linear transformations of function values can be learned alongside function evaluations.

- We demonstrate for the first time that PriorCVAE is agnostic to the type of models that it can approximate by encoding a solution of a system of ordinary differential equations (ODEs).

We provide comparison to different approximate inference methods (Laplace, ADVI, PriorVAE), and showcase our approach on real-world epidemiology data sets.

## 2 BACKGROUND

We provide a concise overview of MCMC as a tool for Bayesian inference in GP models, introduce deep generative models, and summarise VAE and CVAE architectures as required to set up the PriorVAE and  $\pi$ VAE methods.

### 2.1 Markov Chain Monte Carlo and Probabilistic Programming Languages

Under the Bayesian inference paradigm, we are interested in learning the probability distribution of a set of unknown parameters (or latent variables)  $z$  given observed data  $y$ . This is defined by their joint distribution  $p(y, z) = p(y | z) p(z)$ , where  $p(y | z)$  denotes the *likelihood* of the observed data and  $p(z)$  the *prior* for the latent variable  $z$ . Consequently, the *posterior* of the latent variable is expressed as  $p(z | y) \propto p(y | z) p(z)$ .

Markov Chain Monte Carlo (MCMC) is a general sampling technique for sampling from a (possibly) unnormalised target density  $\pi(z)$ , *i.e.* the posterior (Robert et al., 1999; Gelman et al., 1995). MCMC simulates an ergodic Markov chain  $\{z^{(i)}\}_{i \in \mathbb{N}}$  which, under the right conditions, converges to the target distribution  $\pi(z)$ . In practice, the simulation is performed for a finite number of iterations  $N$ , which is sufficiently large to ensure convergence. Diagnostic tools like the R-hat statistic and effective sample size (ESS) metrics aid in assessing the performance and convergence of MCMC (Vehtari et al., 2021). The main advantage of MCMC is the guarantee (under ergodicity conditions) of asymptotic convergence to the target density, which makes MCMC preferable to other methods when our modelling informs decision-making.

Probabilistic programming languages (PPLs, van de Meent et al., 2018; Gordon et al., 2014; Salvatier et al., 2016) abstract MCMC inference algorithms from a user, and allow modellers to focus on model formulation. By automating inference, they significantly lower the cost of iterating model design, leading to a better overall model in a shorter period of time. PPLs also often pro-

vide in-built diagnostics and visualisation tools (Kumar et al., 2019) so users can quickly assess results.

However, MCMC has its limitations. Especially in complex settings, *e.g.* with Gaussian processes or large spatial models, it can be computationally demanding and scales poorly. Simpler inference methods can be useful here, but because PPLs abstract away the visibility to the model internals, this can also pose risks to practical use. We seek to provide a plug&play inference framework used in PPLs as part of large-scale GP modelling or models where a similar approach can provide a remedy.

## 2.2 Auto-encoding Generative Models

Our work hinges on the insight that deep generative models can be used as surrogates in Bayesian modelling. A common shared principle behind generative models (Bond-Taylor et al., 2021; Tomczak, 2022) is to start with samples from the latent distribution, a simple probability distribution such as an i.i.d. Gaussian normal  $z \sim \mathcal{N}(0, I)$ , and apply a generative model in the form of a neural network with trainable parameters to transform the latent distribution into samples from the target distribution. This procedure ensures that the model, during training with samples from the target distribution, learns both the underlying probability structure and the relationship between the generator’s output and the target distribution.

**Variational autoencoders** (VAEs, Kingma and Welling, 2013) are deep generative models with a dual structure: (i) the encoder  $E_\gamma(\cdot)$  maps input  $y \in \mathcal{Y} \subset \mathbb{R}^n$  into a latent space  $\mathcal{Z} \subset \mathbb{R}^d$ , where  $d$  is typically lower than  $n$ ; (ii) the decoder  $D_\psi(\cdot)$  reconstructs this input from the latent representation  $z \in \mathcal{Z}$ . This setup introduces an ‘information bottleneck’, ensuring the latent representation  $z$  encapsulates a compressed version of the input  $y$ .

Unlike traditional autoencoders, a VAE maps  $y$  to a distribution in the latent space, rather than a fixed vector. To facilitate this, VAEs employ variational approximation (Wainwright and Jordan, 2008; Blei et al., 2017; Wainwright et al., 2008) to estimate the posterior distribution:  $p(z|y) \propto p(y|z)p(z)$  and  $p(z|y) \approx q(z|y)$ . Typically, a Gaussian is chosen as the variational family, leading to  $q(z|y) = \mathcal{N}(\mu_z, \sigma_z^2 I_d)$  where  $(\mu_z, \log \sigma_z^2) = E_\gamma(y)$  and  $z \sim \mathcal{N}(\mu_z, \sigma_z^2 I_d)$ . The prior over  $z$ ,  $p(z)$ , remains a standard Gaussian  $\mathcal{N}(0, I_d)$ . As per Kingma and Welling (2013), to achieve optimal encoder and decoder parameters, one maximizes the evidence lower bound or equivalently, minimizes the following loss function:

$$\mathcal{L}_{\text{VAE}} = \mathbb{E}_{q(z|y)} [-\log p(y|z)] + \text{D}_{\text{KL}} [q(z|y) \| p(z)], \quad (1)$$

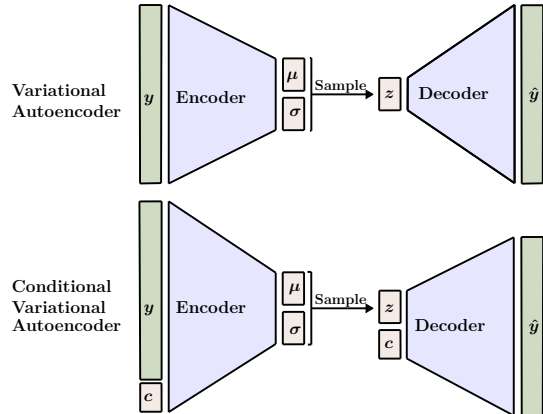


Figure 2: VAE versus CVAE architectures. In CVAE models, both the encoder and decoder get the label  $c$  as input. Traditionally,  $c$  is an observed class label. Here we interpret  $c$  as a hyperparameter of the prior.

where the first component represents the reconstruction quality and the second regularises the difference between the latent variable distribution and its prior.

**Conditional VAEs** (CVAEs, Sohn et al., 2015) extend VAEs by conditioning the generative process on additional information  $c$  (*e.g.*, a class label)—see Fig. 2. This allows CVAEs to handle diverse input–output mappings, as the optimization objective now involves both the data and the conditioning input. This allows us to control the class which we want to generate samples from, and allows the CVAE to learn how to encode and decode separate classes of input differently. The objective for optimisation becomes:

$$\mathcal{L}_{\text{CVAE}} = \mathbb{E}_{q(z|y,c)} [-\log p(y|z,c)] + \text{D}_{\text{KL}} [q(z|y,c) \| p(z|c)]. \quad (2)$$

## 2.3 PriorVAE/ $\pi$ VAE: Encoding Priors

$\pi$ VAE (Mishra et al., 2022) and PriorVAE (Semenova et al., 2022) are two related VAE-based methods that can encode continuous stochastic processes and their finite realisations, respectively. They use the trained decoder as an approximation of computationally complex structures for Bayesian inference with MCMC. In this way, the rigour of MCMC is preserved, enabling inference of complex and expressive models, while these models are scalable due to the simple structure of the VAE’s latent space.  $\pi$ VAE learns low-dimensional embeddings of function classes inspired by the Karhunen–Loève expansion: any stochastic process  $f(s)$  can be represented as an infinite sum  $f(s) = \sum_{j=1}^{\infty} \beta_j \phi_j(s)$ ,

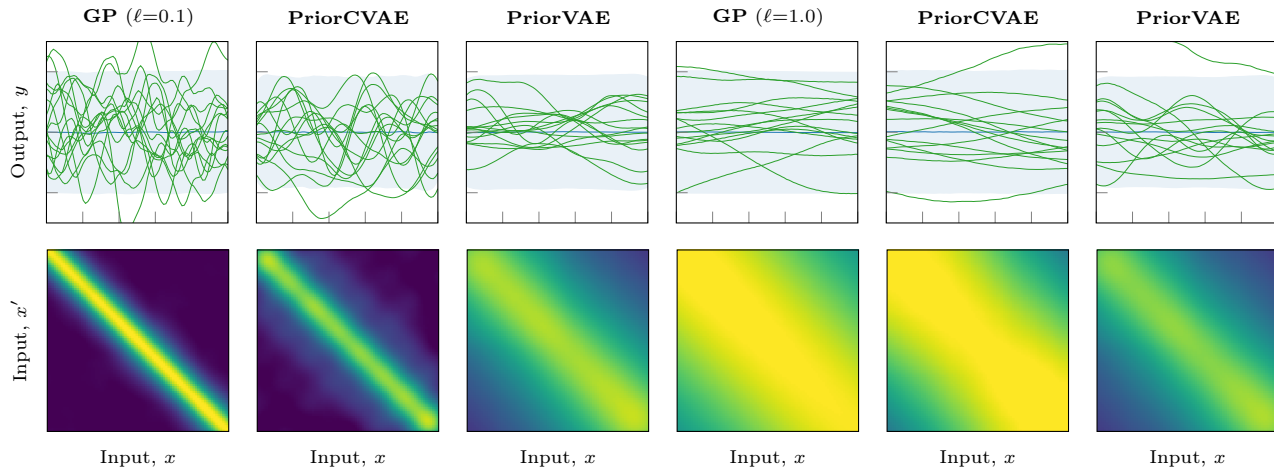


Figure 3: **Our PriorCVAE samples and covariance resemble the original GP.** Example draws (top) and computed Gram (covariance) matrices (bottom, 0 to 1) from a Matérn- $5/2$  prior with lengthscale  $\ell = 0.1$  (three left-hand columns) and  $\ell = 1.0$  (three right-hand columns).

where  $\{\phi_j(\cdot)\}_{j=1}^{\infty}$  is a set of orthonormal basis functions and  $\{\beta_j\}_{j=1}^{\infty}$  are uncorrelated random variables. To train  $\pi$ VAE, the basis functions are learned with a feed-forward neural network over  $s$ , and the random coefficients  $\beta_j$  are encoded using a VAE.

The PriorVAE method was originally proposed as a scalable solution to the small area estimation (SAE) problem in spatial statistics. It encodes finite realisations of a Gaussian process, *i.e.* multivariate normal distributions, which are widely used in spatial statistics. Such distributions are often defined by precision matrices based on the adjacency structure of the modelled areas and include the conditional auto-regressive (CAR), intrinsic conditional auto-regressive (ICAR) and Besag–York–Mollié (BYM) models (Besag, 1974; Besag et al., 1991; Riebler et al., 2016). PriorVAE must be trained on a pre-defined spatial structure, which is a disadvantage compared to  $\pi$ VAE as PriorVAE cannot make predictions at off-grid locations, but is much simpler in common scenarios where the spatial structure is known in advance, as only the VAE needs to be trained, not the feature map. The PriorVAE method is as follows:

1. Fix the spatial structure of interest  $\{x_1, \dots, x_n\}$ , *e.g.* a set of administrative units, or an artificial computational grid.
2. Draw evaluations of a GP prior  $f \sim \mathcal{GP}(\cdot)$  over the spatial structure and train the VAE to approximate these evaluations  $f_{\text{GP}} = (f(x_1), \dots, f(x_n))^{\top}$ .
3. Perform Bayesian inference of the overarching model using MCMC, where  $f_{\text{GP}}$  is approximated using the trained decoder  $D_{\psi}(\cdot)$ :  $f_{\text{GP}} \approx f_{\text{PriorVAE}} = D_{\psi}(z_d)$ ,  $z_d \sim \mathcal{N}(0, I_d)$ .

### 3 METHODS

In this section, we introduce the PriorCVAE method which aims to enable parameter inference by explicitly conditioning the VAE on stochastic process hyperparameters. This enhancement builds upon the strengths of the PriorVAE while addressing its inability to encode hyperparameters.

#### 3.1 Enabling Parameter Inference

While the PriorVAE is effective at encoding priors, it has an inherent limitation: the omission of hyperparameter encoding, which prevents the estimation of hyperparameters during Bayesian inference. This limitation arises because the encoding network,  $E_{\gamma}(f_{\text{GP}})$ , does not distinguish between samples generated using different values of hyperparameters. Similarly, the decoder  $D_{\psi}(z)$  only models  $f_{\text{GP}}$  directly using the variables  $z$ , and no additional condition.

In restricted simple cases this issue can be bypassed. Consider a GP  $f \sim \mathcal{GP}(0, \kappa)$  with a kernel  $\kappa(\cdot, \cdot)$ , where the magnitude (variance) is separable from other model hyperparameters  $\theta$ :  $\kappa(s_i, s_j) = \sigma^2 R_{\theta}(s_i, s_j)$ . Here  $R_{\theta}$  is, for example, the radial basis function kernel (RBF, Broomhead and Lowe, 1988),  $R_{\theta}(s_i, s_j) = \exp(-\|s_i - s_j\|^2 / 2\ell^2)$ , which has one parameter  $\theta = \{\ell\}$ , the lengthscale  $\ell$ . Due to this separability, while training a VAE, it is sufficient to encode ‘standardised’ draws, *i.e.* with  $\sigma = 1$ , so the priors to be encoded are drawn as  $f_{\text{std}} \sim \mathcal{GP}(0, \kappa_{\text{std}})$ , where  $\kappa_{\text{std}}$  is simply  $\kappa_{\text{std}}(s_i, s_j) = R_{\theta}(s_i, s_j)$ . At the inference stage, the magnitude  $\sigma^2$  can be estimated explicitly since  $f = \sigma f_{\text{std}}$ . This trick is not possible in general and even in this specific example, information about the



lengthscale  $\ell$  is lost during the VAE training. The issue is amplified further when working with even more complicated cases, such as non-stationary kernels.

Our solution is a new method called PriorCVAE, pairing the PriorVAE workflow with a CVAE architecture. The encoder and decoder condition on the hyperparameters of the GPs, *i.e.*  $c = \theta$ , allowing us to generate approximate evaluations of the prior for specific hyperparameters, and ultimately to perform inference on hyperparameters. The hyperparameters may be categorical or real-valued, allowing freedom of GP kernel choice.

### 3.2 PriorCVAE Objective

We introduce an additional tuning parameter and use the original probabilistic formulation in the VAE rather than traditional mean squared error (MSE) as the reconstruction loss. The log-likelihood, assuming that the reconstructed sample  $f_{\text{PriorCVAE}}$  is given by  $f_{\text{PriorCVAE}} \sim \mathcal{N}(f_{\text{GP}}, \sigma_{\text{vae}}^2)$ , is

$$-\log \mathcal{N}(f_{\text{GP}}, \sigma_{\text{vae}}^2) = \frac{1}{2\sigma_{\text{vae}}^2} \text{MSE}(f_{\text{GP}}, f_{\text{PriorCVAE}}) + D \log(\sigma_{\text{vae}} \sqrt{2\pi}), \quad (3)$$

where  $D$  is the dimensionality of  $x$ . Previously [Rybkin et al. \(2021\)](#) have shown that  $\mathcal{L} = D \log \sigma_{\text{vae}} + \frac{1}{2\sigma_{\text{vae}}^2} \text{MSE}(f_{\text{GP}}, f_{\text{PriorCVAE}}) + \text{D}_{\text{KL}}[q(z|y) \| p(z)]$  leads to improved results when optimising for  $\sigma_{\text{vae}}$ , but we did not find this approach beneficial.

Instead, we use  $\sigma_{\text{vae}}$  as a hyperparameter, which affects the quantity of uncertainty learned by PriorCVAE, leading to better uncertainty calibration. The log-likelihood can be written as  $-\frac{1}{2\sigma_{\text{vae}}^2} \text{MSE}(f_{\text{GP}}, f_{\text{PriorCVAE}}) + c$ , and the full objective becomes:

$$\mathcal{L}_{\text{PriorCVAE}} = \frac{1}{2\sigma_{\text{vae}}^2} \text{MSE}(f_{\text{GP}} | \theta, f_{\text{PriorCVAE}} | \theta) + \text{D}_{\text{KL}}[\mathcal{N}(\mu_z, \sigma_z^2 I_d | \theta) \| \mathcal{N}(0, I_d)]. \quad (4)$$

Thus,  $\sigma_{\text{vae}}^2$  varies the weighting of the two terms in the loss. This approach is closely related to  $\beta$ -VAE ([Higgins et al., 2017](#)) trained using the objective  $\mathcal{L}_{\beta\text{-VAE}} = \frac{1}{2} \text{MSE}(y, \hat{y}) + \beta \text{D}_{\text{KL}}[q(z|y) \| p(z)]$ , but in our formulation the weighting parameter is interpretable because it is linked to the amplitude of generated samples. The resulting workflow of our PriorCVAE method is presented in [Alg. 1](#).

### 3.3 Outlook

The last step of the PriorCVAE workflow in [Alg. 1](#) highlights why the method is computationally efficient. GP evaluations can be computed as  $f_{\text{GP}} | \theta = L_{\theta} z_n$ ,  $z_n \sim$

---

#### Algorithm 1 PriorCVAE workflow

---

1. Fix the spatial structure of interest  $\{x_1, \dots, x_n\}$  to, *e.g.*, a set of administrative units  $B = \{B_1, \dots, B_n\}$ , or an artificial computational grid  $G = \{g_1, \dots, g_n\}$ .
  2. Draw evaluations of a prior  $f$  over the spatial structure governed by hyperparameters  $\theta$ :  $f \sim \mathcal{GP}_{\theta}(\cdot)$  over  $G$ , or  $f \sim \mathcal{MVN}_{\theta}(\cdot)$  over  $B$ .
  3. Use the vector of realisations  $f_{\text{GP}} = (f(x_1), \dots, f(x_n))^{\top}$  as data for a CVAE to encode, conditional on hyperparameters value  $c = \theta$ . Train PriorCVAE using the loss from [Eq. \(4\)](#).
  4. Perform Bayesian inference with MCMC of the overarching model, including latent variables and hyperparameters  $\theta$ , by approximating  $f_{\text{GP}} | \theta$  with  $f_{\text{PriorCVAE}} | \theta$  in a drop-in manner using the trained decoder  $D_{\psi}(\cdot)$ :  $f_{\text{GP}} | \theta \approx f_{\text{PriorCVAE}} | \theta = D_{\psi}(z_d, \theta)$ ,  $z_d \sim \mathcal{N}(0, I_d)$ .
- 

$\mathcal{N}(0, I_n)$ , where  $L_{\theta}$  is a Cholesky decomposition of the covariance matrix,  $K_{\theta} = L_{\theta} L_{\theta}^{\top}$ . The Cholesky decomposition has  $\mathcal{O}(n^3)$  cost, and must be re-calculated for different values of the parameters  $\theta$  we want to infer.

PriorCVAE, instead, performs a non-linear transformation  $f_{\text{PriorCVAE}} | \theta = D_{\psi}(z_d, \theta)$ , s.t.  $z_d \sim \mathcal{N}(0, I_d)$ , of a smaller vector  $z_d$ , with  $d < n$ . This is efficient to evaluate since, once trained, the parameters  $\psi$  remain static. The primary computational overhead relates to matrix operations within the decoder  $D_{\psi}(\cdot)$ . For instance, for a multilayer perceptron the complexity is  $\mathcal{O}(dhn)$ , where  $h$  is the number of hidden dimensions. In the examples shown in [Sec. 4](#), we use small  $h$ , *e.g.* 1 or 2. Hence, the complexity is  $\mathcal{O}(dn) \leq \mathcal{O}(n^2)$ , providing clear computational advantages.

## 4 EXPERIMENTS

We showcase the capability of the proposed method PriorCVAE in a series of experiments, both in terms of encoding priors efficiently as well as inference and parameter inference. In [Sec. 4.1](#), we experiment with a Gaussian process prior and showcase the capability of PriorCVAE to encode the prior and speed up MCMC inference. In [Sec. 4.2](#), we move to the challenging setup of non-stationary kernels and show the prior encoding capability of PriorCVAE. In [Sec. 4.3](#), we demonstrate the capability of PriorCVAE to encode diffusion process priors. In [Sec. 4.4](#) we demonstrate the method on real-life spatial data of HIV prevalence in Zimbabwe, and, finally, in [Sec. 4.5](#) we demonstrate that applications of

PriorCVAE are not limited by spatial modelling by using the method to encode a solution of the SIR model—an ODE used to model infectious disease dynamics.

#### 4.1 Gaussian Process Prior

We experiment with Gaussian process prior kernels and encode it using both PriorVAE (Semenova et al., 2022) and the proposed model, PriorCVAE. We compare against PriorVAE and show the superior prior encoding capability of PriorCVAE. Then, we move to the inference and parameter inference task and compare against the baseline, GP using MCMC inference.

**Encoding prior** We encode the priors evaluated over a regular one-dimensional grid of  $n=80$  points over the interval  $[0, 1]$ . Training samples are drawn from a GP with zero mean and standardised ( $\sigma^2=1$ ) kernel  $\kappa_\ell^{\text{Matérn-5/2}}$ . The model has the following hierarchical structure with a hyperprior  $\mathcal{U}$  on the lengthscale  $\ell$  of the kernel, which also acts as the condition  $c$  of the CVAE model

$$\begin{cases} \ell & \sim \mathcal{U}(0.01, 0.99), \\ f | \ell & \sim \mathcal{GP}(0, \kappa_\ell^{\text{Matérn-5/2}}(\cdot, \cdot)). \end{cases} \quad (5)$$

App. A provides neural network training details. Fig. 3 showcases three sets of priors: GP, PriorCVAE, and PriorVAE for two lengthscales  $\ell=\{0.1, 1.0\}$ . From the plot, we can observe that the samples from PriorCVAE closely resemble to the GP samples in comparison with PriorVAE whose samples are not dependent on the lengthscale and are thus inflexible. We also present the empirical covariance in Fig. 3.

**MCMC inference** A ground truth curve was generated using the RBF kernel with the lengthscale  $l_{\text{true}} = 0.2$ . To generate observed data, we selected four locations and added a random amount of noise at each of the locations, distributed as  $s \sim \mathcal{N}^+(0.1)$ . We fit three models to this data using the NUTS sampler using the three different priors:  $f_{\text{GP-RBF}}$ ,  $f_{\text{PriorVAE-RBF}}$  and  $f_{\text{PriorCVAE-RBF}}$ . Fig. 4 presents estimated means and Bayesian credible intervals (BCIs) obtained by the three models. All the estimated means are close to each other, but PriorCVAE’s BCIs are much closer to the GP’s BCIs than the BCIs from PriorVAE. All three models were run using 5000 warm-up steps, 50000 post warm-up iterations<sup>3</sup> and three chains. Evaluation of run times, number of effective samples and number of effective samples per second are also presented in Fig. 4. The number of effective steps of PriorCVAE per

<sup>3</sup>PriorVAE and PriorCVAE models require much fewer iterations for convergence. These high values are required for the GP model to converge and, hence, have been set equal for all three models.

second is order of 10K times higher than the one of the original GP model, while the lengthscale parameter can also be recovered. Fig. 4 presents posterior estimates of the lengthscale parameter produced by PriorCVAE and GP models, which are closely matched.

**Comparison with Laplace approximation and ADVI** Using the same implementation software NumPyro (Phan et al., 2019; Bingham et al., 2019) as for the above models, we performed inference using popular approximation techniques - Laplace approximation and automatic differentiation variational inference (ADVI, Kucukelbir et al., 2017). Results presented in Fig. A8 show that ADVI failed at estimating both the mean and the lengthscale; Laplace approximation is able to estimate the mean well, but produced no characterisation of uncertainty, as well as only a point estimate for the lengthscale.

#### Encoding discrete priors and function properties

It is also possible to encode and infer priors over a discrete set of values. Example with a binary prior on the lengthscale is presented in App. B.

Similarly to other prior-encoding VAEs, PriorCVAE is able to encode function properties alongside function realisations. The integral  $\mathcal{I} = \int_D \exp(f(s)) ds, s \in D$  is a crucial quantity required to evaluate log-Gaussian Cox process (LGCP) likelihood (Møller et al., 1998). In App. C we demonstrate how this function property can be learnt with PriorCVAE.

#### 4.2 Encoding Non-stationary Kernels

We show for the first time that prior-encoding VAEs are also able to learn non-stationary GPs. Consider a kernel which is a product of linear and RBF kernels:

$$\begin{aligned} \kappa(s_i, s_j) &= \kappa_{\text{lin}}(s_i, s_j) \kappa_{\text{rbf}}(s_i, s_j) \\ &= (s_i - c_{\text{lin}})^\top (s_j - c_{\text{lin}}) \exp\left(-\frac{\|s_i - s_j\|^2}{2\ell^2}\right). \end{aligned} \quad (6)$$

We fix  $c_{\text{lin}}=0.4$  and aim to encode the lengthscale as the condition. We also set a narrower prior on the lengthscale:  $\ell \sim \mathcal{U}(0.01, 0.4)$ , instead of  $\ell \sim \mathcal{U}(0.01, 0.99)$ , in order to test PriorCVAE’s extrapolation abilities. Training details are reported in App. D. Visual assessment of the quality of the learned priors is presented in Fig. 6, which corresponds to lengthscales  $\ell=0.05$  and  $\ell=0.2$  contained in the  $(0.01, 0.4)$  interval along with the empirical covariance matrices.

**Extrapolation of hyperparameters** Even though we only trained the decoder with lengthscales drawn from  $(0.01, 0.4)$  interval, it is possible to condition PriorCVAE draws on lengthscales  $\ell$  which lie outside

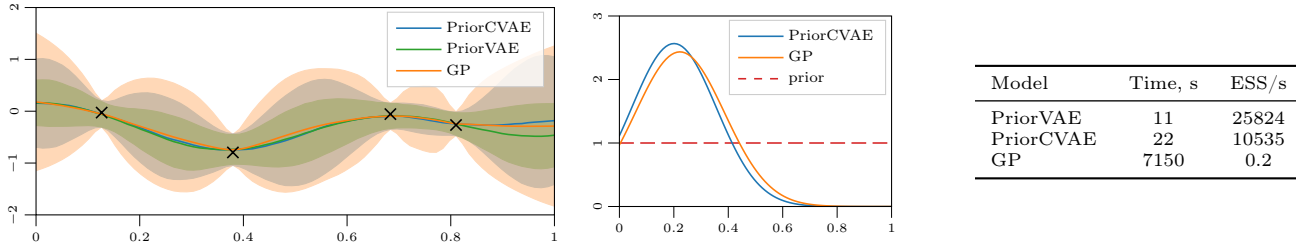


Figure 4: MCMC inference comparison between PriorCVAE, PriorVAE, and GP. Left: Estimated means and uncertainty bounds obtained by the three models; PriorCVAE is much closer to the baseline(GP) than PriorVAE. Middle: Lengthscale posteriors of the GP and PriorCVAE model. Right: Comparison of inference statistics.

of this interval. Fig. A17 compares the quality of extrapolation for  $\ell = 0.5$  and  $\ell = 0.9$ , showing that the prior quality is high close to the interval, and deteriorates for  $\ell$  further away.

### 4.3 Encoding diffusion processes

We experiment with encoding priors of a diffusion process (DP) double-well, which is defined by an SDE:

$$dx_t = \theta_1 x_t (\theta_2 - x_t^2) + d\beta_t, \quad (7)$$

with  $\theta_1, \theta_2$  being the parameters of the DP and  $Q$  is the spectral density. The marginal state distributions have two modes that sample state trajectories keep visiting through time. In App. G, we discuss the setup and show how the proposed PriorCVAE model can also be used to encode the DP priors, which can then be used to speed-up inference in a model with such DP prior.

### 4.4 HIV Prevalence in Zimbabwe

We consider household survey data from the 2015 to 2016 Population-based HIV Impact Assessment Survey in Zimbabwe (Sachathep et al., 2021). The observed positive cases  $y_i$  among all observed cases  $n_i$  in each administrative unit  $B_i, i = \{1, \dots, 63\}$  are modelled as follows:  $y_i \sim \text{Binomial}(n_i, \theta_i)$ ,  $\text{logit}^{-1}(\theta_i) = b_0 + f_i$ ,  $f \sim \text{MVN}(0, K)$ ,  $\kappa_{ij} = \sigma^2 \exp\left(-\frac{\|c_i - c_j\|^2}{2\ell^2}\right)$ ,  $b_0 \sim \mathcal{N}(0, 1)$ ,  $\ell \sim \text{Gamma}(2, 4)$ , and  $\sigma \sim \text{Gamma}(1.5, 1.5)$ . Here  $\theta_i$  is the estimate of HIV prevalence in unit  $i$ , and  $\phi = (f_1, \dots, f_{63})$  is the spatial random effect, a GP with RBF kernel evaluated at the centroids of  $B_i$ . Neural network training details are available in App. E.

**MCMC inference** We performed inference using both the original GP prior  $f_{\text{GP}}$  and the trained  $f_{\text{PriorCVAE}}$  for  $\phi$ . MCMC inference was performed using  $n_{\text{warmup}} = 2000$  burn-in steps, and  $n_{\text{samples}} = 10000$  post-warmup steps with the NUTS sampler. Run times and sampling efficiency are presented in Table on Fig. 1. Estimates of parameters  $\ell$  and  $\sigma$  are shown on Fig. A18, comparison of estimated prevalence obtained using the original

$f_{\text{GP}}$  prior, and the model with the  $f_{\text{PriorCVAE}}$  prior are presented on Fig. A19 and resulting maps of estimated prevalence are presented on Fig. 1.

**Comparison with R-INLA** R-INLA (Lindgren and Rue, 2015) is a popular software for Bayesian spatial modelling and is viewed as state-of-the-art in many applied fields. While being very fast, R-INLA has limitations, such as, for example, it does not permit the RBF kernel, or Matérn kernels with smoothness higher than  $\nu = \alpha - m/2$ , where  $\alpha \in (0, 2]$  and  $m$  is space dimensionality. We discuss the comparison of the proposed PriorCVAE tool with R-INLA in App. E.

### 4.5 Encoding ODE Solutions: SIR Example

All of the previous examples were concerned with encoding GP priors. In this section we demonstrate that also ODE solutions can be encoded using the same technique on the example of the SIR model. The SIR model is a classical model from mathematical epidemiology (Kermack and McKendrick, 1927) that divides a population into three compartments (Susceptible, Infected, and Recovered) to study the spread of infectious diseases by modelling time-dependent volumes of compartments as solutions of a system of differential equations:

$$\dot{S} = -\beta \cdot \frac{S \cdot I}{N}, \quad \dot{I} = \beta \cdot \frac{S \cdot I}{N} - \gamma \cdot I, \quad \dot{R} = \gamma \cdot I.$$

Here  $S$  is the number of susceptible individuals,  $I$  is the number of infected individuals,  $R$  is number of recovered individuals,  $N$  is the total population size,  $\beta$  is the transmission rate and  $\gamma$  is the recovery rate.

**Encoding priors** Initial datum  $(S_0, I_0, R_0)$  and parameters  $\beta, \gamma$  define a unique solution of the ODE. Inference is then performed by matching observed number of infected individuals  $y(t)$  and the expected number of infected individuals  $I(t)$  via, for example, a count distribution, such as Poisson or Negative Binomial:  $y(t) \sim \text{NegBin}(I(t), \phi)$ , where  $\phi$  is the overdispersion parameter. We rely in this example on the data of influenza A (H1N1) outbreak in 1978 at a British boarding school. The data consists of the daily number of

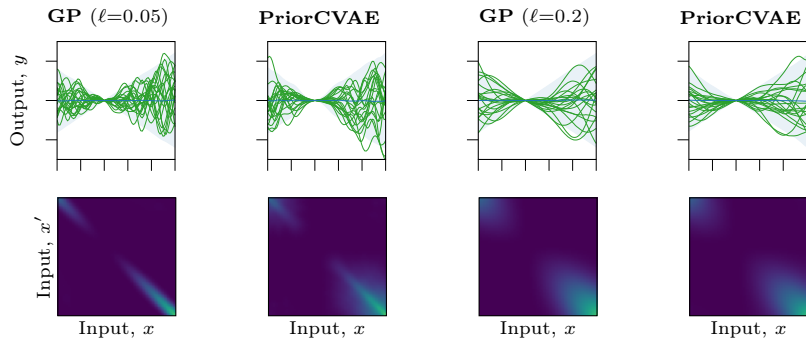
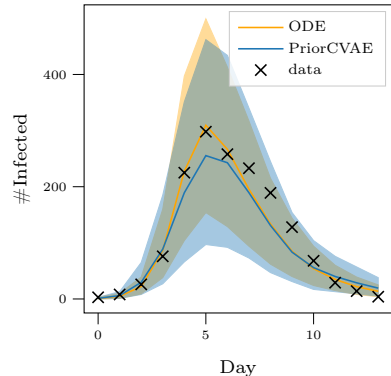


Figure 5: Influenza outbreak SIR. Figure 6: Non-stationary kernel: Example draws (top) from the GP model: PriorCVAE model gives inference similar to the exact ODE solution. and the PriorCVAE model, and empirical covariance matrices (bottom row) with lengthscale  $\ell = 0.05$  (two left-hand columns) and  $\ell = 0.2$  (two right-hand columns).

students in bed, spanning over a time interval of 14 days. There were  $N=763$  male students and it is reported that one infected boy started the epidemic  $I_0 = 1$ . The data are freely available in the R package *outbreaks*, maintained as part of the R Epidemics Consortium.

**PriorCVAE training** Since ODE solution is unique given the initial conditions, and only one compartment ( $I$ ) is used for inference, it is sufficient to train the neural network on the draws of  $I(t)$ . Since  $I(t)$  needs to lie between 0 and  $N$ , at the last layer we apply the sigmoid activation function and multiply the result by  $N$ . For training details see App. F. Fig. A20 demonstrates the family of learnt trajectories of the infected compartment parameterised by the condition  $c=(\beta, \gamma)$ .

**MCMC inference** For inference, we used the same priors as in Grinsztajn et al. (2021):  $\beta \sim \mathcal{N}^+(2, 1)$ ,  $\gamma \sim \mathcal{N}^+(0.4, 0.5)$ ,  $\phi^{-1} \sim \text{Exp}(5)$  and initial datum  $(S_0, I_0, R_0) = (N - 1, 1, 0)$ . Fig. 5 shows inference results under the original and PriorCVAE-based models and Fig. A21 shows parameter estimates.

## 5 DISCUSSION AND CONCLUSION

In this paper, we introduce PriorCVAE, a method based on deep generative modelling that enables explicit parameter estimation while performing fast and efficient MCMC inference. It covers a gap in the literature on encoding finite evaluations of stochastic processes, where previous methods lost information about underlying parameters. We solve the problem by conditioning the generative process on the parameters of interest and demonstrate that the conditioning can be performed both by categorical and continuous parameters. PriorCVAE does this while retaining the advantages of PriorVAE at the inference stage, *i.e.* much shorter computation times and higher effective samples size than an equivalent model fully inferred with MCMC.

Side-by-side comparison of the GP, PriorVAE, and PriorCVAE models has shown that although PriorCVAE is less efficient than PriorVAE, it can better reconstruct the underlying model; furthermore, the number of effective steps per second achieved by PriorCVAE is still about 10K higher than for the GP. Using non-stationary GP example, we demonstrated that it is possible to perform extrapolation with respect to hyperparameters; that the quality of reconstructed priors remains high if the out-of-sample hyperparameter values are close to those in-sample and the quality of reconstruction deteriorates with distance. We quantified the quality of the learnt PriorVAE and PriorCVAE priors by measuring distance of their empirical covariance matrices to the one of the original GP prior. Table A1 showed that this form of quantification agrees with the results obtained at inference, *i.e.* that PriorCVAE priors match GP priors better than PriorVAE. Future work includes variations in the reconstruction loss, using, for example, Frobenius norm or maximum mean discrepancy (Gretton et al., 2012) to match higher moments by design. PriorCVAE is kernel-agnostic, which gives it a serious competitive advantage over state-of-the-art methods such as R-INLA (Rue et al., 2017), which only allows Matérn kernels of smoothness up to  $\nu=1$  in two dimensions, not RBF kernels or products of non-Matérn kernels.

In the final example, we demonstrate that PriorCVAE is agnostic not only to the kernel of a GP, but to the prior model as a whole. This model can be of mechanistic nature, such as a system of differential equations.

The key features of PriorCVAE — speed, efficiency, and ability to estimate parameters within MCMC — have great potential to make a major impact in spatial statistics and related domains requiring inference over correlated structures. Immediate potential applications include time series, as well as a wider array of kernels.



## References

- S. D. Axen, A. Gessner, C. Sommer, N. Weitzel, and Á. Tejero-Cantero. Spatiotemporal modeling of European paleoclimate using doubly sparse Gaussian processes. *arXiv preprint arXiv:2211.08160*, 2022.
- S. Belda, L. Pipia, E. Amin, M. Salinero, P. Reyes, and J. Verrelst. Crop phenology retrieval through Gaussian process regression. In *2021 IEEE International Geoscience and Remote Sensing Symposium IGARSS*, pages 6256–6259. IEEE, 2021.
- J. Besag. Spatial interaction and the statistical analysis of lattice systems. *Journal of the Royal Statistical Society: Series B (Methodological)*, 36(2):192–225, 1974.
- J. Besag, J. York, and A. Mollié. Bayesian image restoration, with two applications in spatial statistics. *Annals of the Institute of Statistical Mathematics*, 43(1):1–20, 1991.
- E. Bingham, J. P. Chen, M. Jankowiak, F. Obermeyer, N. Pradhan, T. Karaletsos, R. Singh, P. A. Szerlip, P. Horsfall, and N. D. Goodman. Pyro: Deep universal probabilistic programming. *Journal of Machine Learning Research*, 20:28:1–28:6, 2019.
- D. M. Blei, A. Kucukelbir, and J. D. McAuliffe. Variational inference: A review for statisticians. *Journal of the American Statistical Association*, 112(518):859–877, 2017.
- S. Bond-Taylor, A. Leach, Y. Long, and C. G. Willcocks. Deep generative modelling: A comparative review of VAEs, GANs, normalizing flows, energy-based and autoregressive models. *arXiv preprint arXiv:2103.04922*, 2021.
- J. Bradbury, R. Frostig, P. Hawkins, M. J. Johnson, C. Leary, D. Maclaurin, G. Necula, A. Paszke, J. VanderPlas, S. Wanderman-Milne, and Q. Zhang. JAX: composable transformations of Python+NumPy programs, 2018. URL <http://github.com/google/jax>.
- D. S. Broomhead and D. Lowe. Radial basis functions, multi-variable functional interpolation and adaptive networks. Technical report, Royal Signals and Radar Establishment Malvern (United Kingdom), 1988.
- B. Carpenter, A. Gelman, M. D. Hoffman, D. Lee, B. Goodrich, M. Betancourt, M. Brubaker, J. Guo, P. Li, and A. Riddell. Stan: A probabilistic programming language. *Journal of statistical software*, 76(1), 2017.
- T. Dai, S. M. Jordaan, and A. P. Wemhoff. Gaussian process regression as a replicable, streamlined approach to inventory and uncertainty analysis in life cycle assessment. *Environmental Science & Technology*, 56(6):3821–3829, 2022.
- M. P. Deisenroth, D. Fox, and C. E. Rasmussen. Gaussian processes for data-efficient learning in robotics and control. *IEEE Transactions on Pattern Analysis and Machine Intelligence*, 37(2):408–423, 2013.
- A. Doucet. A note on efficient conditional simulation of Gaussian distributions. Technical report, Departments of Computer Science and Statistics, University of British Columbia, 2010.
- A. Gelman, J. B. Carlin, H. S. Stern, and D. B. Rubin. *Bayesian Data Analysis*. Chapman and Hall/CRC, 1995.
- A. D. Gordon, T. A. Henzinger, A. V. Nori, and S. K. Rajamani. Probabilistic programming. In *Future of Software Engineering Proceedings*, pages 167–181. 2014.
- A. Gretton, K. M. Borgwardt, M. J. Rasch, B. Schölkopf, and A. Smola. A kernel two-sample test. *The Journal of Machine Learning Research*, 13(1):723–773, 2012.
- L. Grinsztajn, E. Semanova, C. C. Margossian, and J. Riou. Bayesian workflow for disease transmission modeling in stan. *Statistics in Medicine*, 40(27):6209–6234, 2021.
- I. Higgins, L. Matthey, A. Pal, C. Burgess, X. Glorot, M. Botvinick, S. Mohamed, and A. Lerchner. beta-VAE: Learning basic visual concepts with a constrained variational framework. In *International Conference on Learning Representations*, 2017.
- M. D. Hoffman and A. Gelman. The no-u-turn sampler: Adaptively setting path lengths in hamiltonian monte carlo. *Journal of Machine Learning Research*, 15(47):1593–1623, 2014. URL <http://jmlr.org/papers/v15/hoffman14a.html>.
- W. O. Kermack and A. G. McKendrick. A contribution to the mathematical theory of epidemics. *Proceedings of the Royal Society of London. Series A, Containing Papers of a Mathematical and Physical Character*, 115(772):700–721, 1927.
- D. P. Kingma and J. Ba. Adam: A method for stochastic optimization. *arXiv preprint arXiv:1412.6980*, 2014.
- D. P. Kingma and M. Welling. Auto-encoding variational Bayes. *arXiv preprint arXiv:1312.6114*, 2013.
- A. Krause and C. Guestrin. Nonmyopic active learning of Gaussian processes: an exploration-exploitation approach. In *Proceedings of the 24th International Conference on Machine Learning*, pages 449–456, 2007.
- A. Kucukelbir, D. Tran, R. Ranganath, A. Gelman, and D. M. Blei. Automatic differentiation variational inference. *Journal of Machine Learning Research*, 2017.
- R. Kumar, C. Carroll, A. Hartikainen, and O. Martin. Arviz a unified library for exploratory analysis of Bayesian models in python. *Journal of Open Source Software*, 4(33):1143, 2019.
- F. Lindgren and H. Rue. Bayesian spatial modelling with r-inla. *Journal of Statistical Software*, 63(19), 2015.
- S. Mishra, S. Flaxman, T. Berah, M. Pakkanen, H. Zhu, and S. Bhatt. *pi* vae: Encoding stochastic process priors with variational autoencoders. *Statistics & Computing*, 2022.
- J. Møller, A. R. Syversveen, and R. P. Waagepetersen. Log Gaussian cox processes. *Scandinavian journal of statistics*, 25(3):451–482, 1998.
- O. Obrezanova, G. Csányi, J. M. Gola, and M. D. Segall. Gaussian processes: a method for automatic qsar modeling of adme properties. *Journal of Chemical Information and Modeling*, 47(5):1847–1857, 2007.
- A.-P. Oriol, A. Virgile, C. Colin, D. Larry, F. C. J., K. Maxim, K. Ravin, L. Jupeng, L. C. C., M. O. A., O. Michael, V. Ricardo, W. Thomas, and Z. Robert. Pymc: A modern and comprehensive probabilistic programming framework in python. *PeerJ Computer Science*, 9:e1516, 2023.
- D. Phan, N. Pradhan, and M. Jankowiak. Composable effects for flexible and accelerated probabilistic programming in numpyro. *arXiv preprint arXiv:1912.11554*, 2019.
- A. Riebler, S. H. Sørbye, D. Simpson, and H. Rue. An intuitive Bayesian spatial model for disease mapping

- that accounts for scaling. *Statistical Methods in Medical Research*, 25(4):1145–1165, 2016.
- C. P. Robert, G. Casella, and G. Casella. *Monte Carlo Statistical Methods*, volume 2. Springer, 1999.
- H. Rue, A. Riebler, S. H. Sørbye, J. B. Illian, D. P. Simpson, and F. K. Lindgren. Bayesian computing with inla: a review. *Annual Review of Statistics and Its Application*, 4:395–421, 2017.
- O. Rybkin, K. Daniilidis, and S. Levine. Simple and effective vae training with calibrated decoders. In *International Conference on Machine Learning*, pages 9179–9189. PMLR, 2021.
- K. Sachatp, E. Radin, W. Hladik, A. Hakim, S. Saito, J. Burnett, K. Brown, N. Phillip, S. Jonnalagadda, A. Low, et al. Population-based HIV Impact Assessments (PHIA) Survey Methods, Response, and Quality in Zimbabwe, Malawi, and Zambia. *Journal of Acquired Immune Deficiency Syndromes (1999)*, 87(Suppl 1):S6, 2021.
- J. Salvatier, T. V. Wiecki, and C. Fonnesbeck. Probabilistic programming in Python using PyMC3. *PeerJ Computer Science*, 2:e55, 2016.
- T. S. Schroeter, A. Schwaighofer, S. Mika, A. Ter Laak, D. Suelzle, U. Ganzer, N. Heinrich, and K.-R. Müller. Predicting lipophilicity of drug-discovery molecules using Gaussian process models. *ChemMedChem: Chemistry Enabling Drug Discovery*, 2(9):1265–1267, 2007.
- E. Semenova, M. L. Guerriero, B. Zhang, A. Hock, P. Hopcroft, G. Kadamur, A. M. Afzal, and S. E. Lazic. Flexible fitting of protac concentration–response curves with changepoint Gaussian processes. *SLAS DISCOVERY: Advancing the Science of Drug Discovery*, 26(9):1212–1224, 2021.
- E. Semenova, Y. Xu, A. Howes, T. Rashid, S. Bhatt, S. Mishra, and S. Flaxman. PriorVAE: Encoding spatial priors with variational autoencoders for small-area estimation. *Journal of the Royal Society Interface*, 19(191):20220094, 2022.
- Y. Shapovalova, T. Heskes, and T. Dijkstra. Non-parametric synergy modeling of chemical compounds with Gaussian processes. *BMC bioinformatics*, 23:1–30, 2022.
- K. Sohn, H. Lee, and X. Yan. Learning structured output representation using deep conditional generative models. *Advances in Neural Information Processing Systems*, 28, 2015.
- E. Štrumbelj, A. Bouchard-Côté, J. Corander, A. Gelman, H. Rue, L. Murray, H. Pesonen, M. Plummer, and A. Vehtari. Past, present, and future of software for Bayesian inference. 2023.
- J. M. Tomczak. Deep generative modeling for neural compression. In *Deep Generative Modeling*, pages 173–188. Springer, 2022.
- J.-W. van de Meent, B. Paige, H. Yang, and F. Wood. An introduction to probabilistic programming. *arXiv preprint arXiv:1809.10756*, 2018.
- A. Vehtari, A. Gelman, D. Simpson, B. Carpenter, and P.-C. Bürkner. Rank-normalization, folding, and localization: an improved R for assessing convergence of MCMC (with discussion). *Bayesian Analysis*, 16(2):667–718, 2021.
- M. J. Wainwright and M. I. Jordan. Introduction to variational methods for graphical models. *Foundations and Trends in Machine Learning*, 1:1–103, 2008.
- M. J. Wainwright, M. I. Jordan, et al. Graphical models, exponential families, and variational inference. *Foundations and Trends in Machine Learning*, 1(1–2):1–305, 2008.
- C. K. Williams and C. E. Rasmussen. *Gaussian Processes for Machine Learning*. Number 3. MIT Press, Cambridge, MA, 2006.
- J. You, X. Li, M. Low, D. Lobell, and S. Ermon. Deep Gaussian process for crop yield prediction based on remote sensing data. In *Thirty-First AAAI conference on artificial intelligence*, 2017.
- G. Zhou. Mixed Hamiltonian Monte Carlo for mixed discrete and continuous variables. *Advances in Neural Information Processing Systems*, 33:17094–17104, 2020.

---

# PriorCVAE: Scalable MCMC Parameter Inference with Bayesian Deep Generative Modelling: Supplementary Materials

---

This Supplementary document is organised as follows. [A](#) provides details of continuous condition PriorVAE and PriorCVAE models. [App. B](#) demonstrates example of a binary prior on the GP lengthscale. [App. C](#) demonstrates how to encode integral of the intensity function of the log-Gaussian Cox process. [App. D](#) provides details of the example with non-stationary kernels. [App. E](#) covers details of the real-life data example of HIV Prevalence in Zimbabwe Estimation, including comparison of MCMC, PriorCVAE and R-INLA results. [App. F](#) and [App. G](#) describe details of models encoding SIR and double-well trajectories, correspondingly. [App. H](#) explains software, hardware and reproducibility details. [App. I](#) shows a sample NumPyro code. [App. J](#) contains supplementary figures.

## A Continuous Condition PriorVAE and PriorCVAE: Experiment Details

### Model for priors

$$\begin{cases} \ell & \sim \mathcal{U}(0.01, 0.99), \\ f | \ell & \sim \mathcal{GP}(0, \kappa_\ell^{\text{RBF}}(\cdot, \cdot)). \end{cases} \quad (\text{A8})$$

**Training PriorVAE and PriorCVAE.** We create training and test datasets, each of 100000 randomly sampled GP prior evaluations according to Equations [A8](#). In order to perform one-to-one comparison of PriorVAE and PriorCVAE we opt to keep the train and test sets fixed (as opposed to generating data on the fly during the training process). The architecture of the two models is also identical: both the encoder and the decoder are MLPs with one hidden layer and  $n_{\text{input}} = 80$  input (output for the decoder) nodes,  $n_{\text{h}} = 60$  hidden nodes, and the dimension of the latent space is  $n_{\text{z}} = 40$ . Both models were trained for  $n_{\text{epochs}} = 500$  epochs, with  $n_{\text{batch}} = 2000$  batch size, and  $1e^{-3}$  learning rate using the Adam optimiser. Comparing the training and test losses already provides insights into which model can describe the data better ([Fig. A13](#)): both the test and training losses of PriorCVAE are lower than those for PriorVAE throughout the training process.

Table A1: Quantification of the quality of the learned priors: Frobenius norms measure the distance between empirical covariance matrices obtained from the original GP prior, and learned PriorVAE and PriorCVAE priors  $F_{\text{PriorVAE}} = \|\mathbf{K}_{\text{GP}} - \mathbf{K}_{\text{PriorVAE}}\|_F$ ,  $F_{\text{PriorCVAE}} = \|\mathbf{K}_{\text{GP}} - \mathbf{K}_{\text{PriorCVAE}}\|_F$ .

lengthscale $c = \ell$	0.05	0.1	0.3	0.9
$F_{\text{PriorVAE}}$	45.47	37.48	8.29	22.94
$F_{\text{PriorCVAE}}$	14.45	7.63	6.42	1.99

## B Encoding Lengthscale of a GP as a Binary Condition: experiment details

### Model for priors

$$\begin{cases} c & \sim \text{Bernoulli}(0.5), \\ \ell | c & = (1 - c)\ell_1 + c\ell_2, \\ f | \ell & \sim \mathcal{GP}(0, \kappa_\ell^{\text{RBF}}(\cdot, \cdot)) \end{cases} \quad (\text{A9})$$

**Neural network training details.** We create training and test datasets, each of 100000 randomly sampled GP prior evaluations according to Equations [A9](#). We follow the architecture used in [Semenova et al. \(2022\)](#), i.e. a

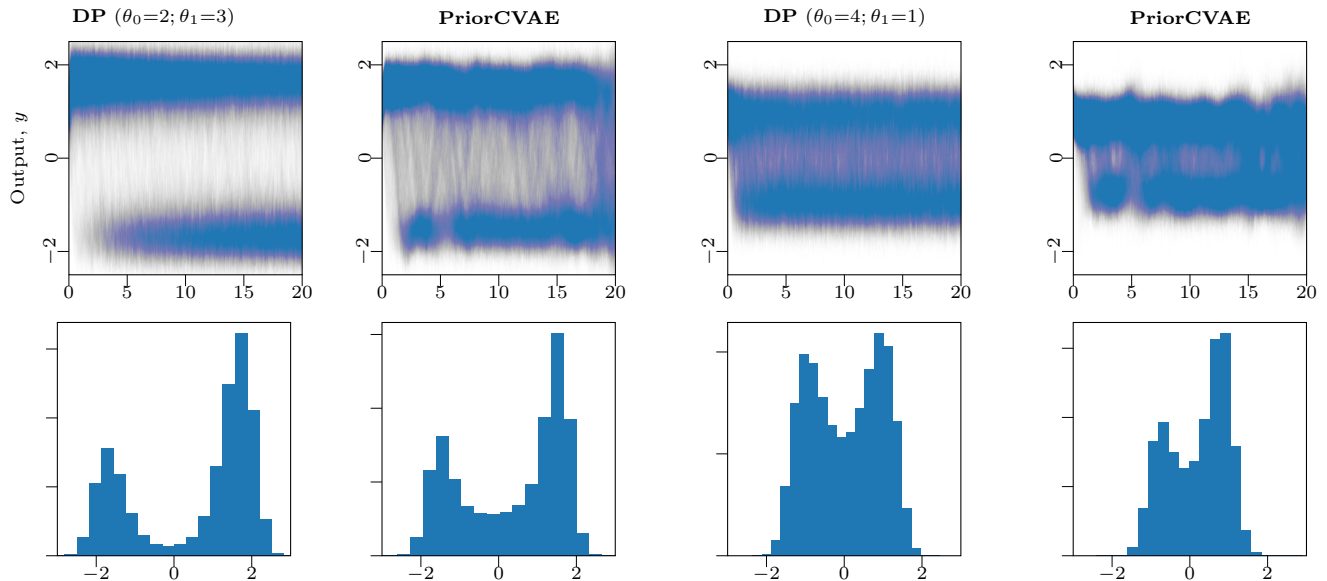


Figure A7: **Encoding diffusion process prior:** (Top) Samples of the Double-Well diffusion process of the true diffusion process and the trained PriorCVAE model for different values of  $\theta$ . (Bottom) The histogram of the samples showing the two wells of the process.

multilayer perceptron (MLP). However, our experiments showed that even one hidden layer is enough to achieve performance similar to the one with two or more hidden layers under this architecture. Both the encoder and the decoder are MLPs and contain one hidden layer of  $n_h = 70$  nodes, and the dimension of the latent space is  $n_z = 50$ . Note, of course, that the input layer of the encoder and the output layer of the encoder both have  $n_{\text{input}} = 100$  nodes, the same size as  $x$ . The model was trained for  $n_{\text{epochs}} = 250$  epochs, with  $n_{\text{batch}} = 1000$  prior evaluations in each batch, and a learning rate of  $1e^{-3}$ , using the Adam optimiser (Kingma and Ba, 2014). The  $\sigma_{\text{vae}}^2$  hyperparameter was set to 0.9. Training of the neural network took 9 minutes<sup>4</sup>.

**MCMC Inference.** To perform inference, we generate one GP realisation according to the true value of the condition  $c = 1$  and use it as the ground truth  $f_{\text{true}}$ . Seven observed data points are sampled by adding i.i.d. noise to the ground truth:  $f_{\text{obs}} \sim \mathcal{N}(f_{\text{true}}, s)$ , where the standard deviation of the noise is modelled with a half-Normal prior  $s \sim \mathcal{N}^+(0.1)$ . Using this observed data we aim to reconstruct the underlying true curve according to three different scenarios: (a) assuming an incorrect condition is known, (b) assuming a known and true condition, and (c) inferring the condition alongside reconstruction of the true trajectory. For all scenarios, we ran 4 MCMC chains with  $n_{\text{warmup}} = 1000$  burn-in steps, and  $n_{\text{samples}} = 100000$  post-warmup steps. Results of scenarios (a) and (b) are presented in Fig. A15; inference in both cases was performed using a NUTS sampler (Hoffman and Gelman, 2014) and took 8 seconds and 30 seconds, correspondingly. Scenario (c) needs a separate treatment as direct inference of discrete parameters, such as  $c \in \{0, 1\}$ , is impossible with NUTS. Instead, we use two alternative approaches. The first approach is to approximate the discrete distribution of the condition with a Beta-prior  $c \sim \text{Beta}(10^{-4}, 10^{-4})$  which is concentrated around values 0 and 1 and assigns low probability away from 0 and 1. This model is inferred using NUTS (see Fig. A14, left) and took 24 seconds to run. The second approach is to assign  $c$  its original discrete prior  $c \sim \text{Bernoulli}(0.5)$  and use the MixedHMC sampler (Zhou, 2020) (see Fig. A14, right); it took 9 minutes to run. The results are very close to those when the true condition value is known (Fig. A14, left), and the posterior samples of  $c$  obtained using the two approaches are shown on the bottom of Fig. A14.

<sup>4</sup>See Section H for hardware details.



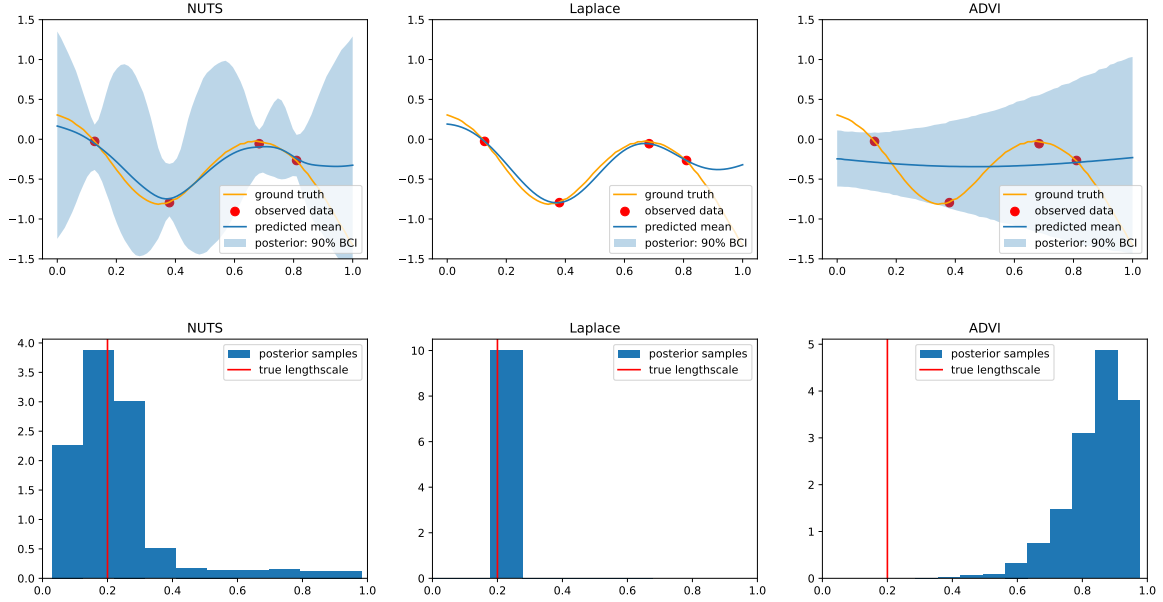


Figure A8: Comparing NUTS, Laplace and ADVI inference results on a one-dimensional Gaussian Process. Top: inferred mean and 90% BCI, bottom: inferred lengthscale. Note, that results of the Laplace approximation and ADVI differ between hardware. See Fig. A11 and Fig. A12 for results obtained on Google Colab.

## C Encoding Integral of the Intensity Function of the Log-Gaussian Cox Process

Similarly to other prior-encoding VAEs, PriorCVAE is able to encode function properties alongside function realisations. The integral

$$\mathcal{I} = \int_D \exp(f(s)) ds, s \in D \quad (\text{A10})$$

is a crucial quantity required to evaluate log-Gaussian Cox process (LGCP) likelihood (Møller et al., 1998).

LGCP is defined by an intensity function

$$\lambda(s) = \exp(f(s)), \quad f(s) \sim \mathcal{GP}(\cdot, \cdot) \quad (\text{A11})$$

which is Gaussian on the log-scale. The log-likelihood of an observed point pattern  $S$ , *i.e.* a collection of observed event locations  $S = \{s_1, s_2, \dots, s_N\}, s_j \in D$ , can then be written as  $L(\lambda|s_1, s_2, \dots, s_N) = \exp(-\int_D \lambda(s) ds) \prod_{j=1}^N \lambda(s_j)$ . Therefore, the log-likelihood involves the integral of the intensity function over the whole observation domain  $\mathcal{I} := \int_D \lambda(s) ds = \int_D \exp(f(s)) ds$ . The presence of this term makes LGCP inference challenging. Here we demonstrate in one-dimensional case  $D = (0, 1)$  that the integral  $\mathcal{I}$  can be encoded jointly with the GP realisations and recovered at inference. For computational stability, we used the following scheme

$$\begin{aligned} \log(\mathcal{I}) &\approx -\log n + \log \left( \sum_{i=1}^n \exp(f(x_i)) \right), \\ &= -\log n + \log\text{-sum-exp}(f(x_i)). \end{aligned} \quad (\text{A12})$$

Here  $\log\text{-sum-exp}(v) = \log(\sum_{i=1}^n \exp(v_i)) = \max(v) + \log[\sum_{i=1}^n \exp(v_i - \max(v))]$ . The objective now includes an additional term - reconstruction loss of the integral value:

$$\begin{aligned} \mathcal{L}_{\text{PriorCVAE}} &= \frac{1}{2\sigma_{f,\text{VAE}}^2} \text{MSE}(f_{\text{GP}}, f_{\text{PriorCVAE}}) + \frac{1}{2\sigma_{\mathcal{I},\text{VAE}}^2} \text{MSE}(\mathcal{I}_{\text{GP}}, \mathcal{I}_{\text{PriorCVAE}}) \\ &\quad - \text{D}_{\text{KL}}[\mathcal{N}(\mu_z, \sigma_z^2 I_d) \parallel \mathcal{N}(0, I_d)], \end{aligned} \quad (\text{A13})$$

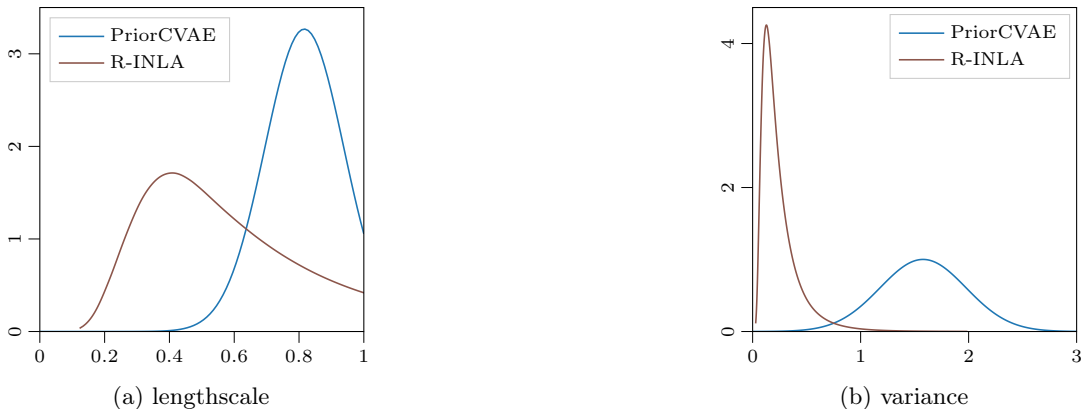


Figure A9: **Zimbabwe experiment:** Parameter estimates produced by R-INLA and PriorCVAE.

where  $\mathcal{I}_{\text{GP}} \approx \frac{1}{n} \sum_{i=1}^n f_{\text{GP}}^i$ ,  $f_{\text{GP}}^i = f(g_i)$ ,  $\{g_i\}_{i=1}^n$  is the computational grid,  $\mathcal{I}_{\text{PriorCVAE}} \approx \frac{1}{n} \sum_{i=1}^n f_{\text{PriorCVAE}}^i$ , and  $\sigma_{f,\text{VAE}}$  and  $\sigma_{\mathcal{I},\text{VAE}}$  are two different tuning parameters.

In this experiment we have focused on GP samples with RBF kernel and  $\ell = 0.2$ . To assess the quality of the integral estimation by the decoder, we compare  $\mathcal{I}_{\text{PriorCVAE}}$  with the value of the integral computed from the recovered  $f_{\text{PriorCVAE}}$  samples. The benefit of such encoding is that if a more complex quadrature is required, it would be performed prior to inference and not during it, even if the evaluations  $f_{\text{GP}}$  are no longer costly. We fix one curve for which we know the true value of the integral computed via the same quadrature rule. Then we iterate through the number of observed points from 5 to 70 in increments of 5 points, and fit the PriorCVAE model to the data five times. Results are presented on Fig. A16. For any assessed number of observed points, the mean estimates produced by the two approaches differ by at most 0.1. The same statement holds for uncertainty intervals. Here, we used the simplest quadrature scheme, however, other quadratures could be used, without adding extra computational cost to the inference step.

## D Encoding Non-stationary Kernels: Experiment Details

**Neural network training details.** CVAE architecture is identical to the two experimentst above. The neural network was trained for  $n_{\text{epochs}} = 5000$  epochs, with  $n_{\text{batch}} = 2000$  batch size, and  $1e^{-3}$  learning rate. Value of the  $\sigma_{\text{vae}}^2$  hyperparameter was set to 0.01.

## E HIV Prevalence in Zimbabwe Estimation

### Inference model

$$\begin{aligned}
 y_i &\sim \text{Binomial}(n_i, \theta_i), \\
 \text{logit}^{-1}(\theta_i) &= f_i, \\
 f &\sim \mathcal{MVN}(0, \mathbf{K}), \\
 \kappa_{ij} &= \text{Matérn}^{1/2}(x_i, x_j), \\
 \ell &\sim \text{Uniform}(0, 1), \sigma \sim \text{Gamma}(1.5, 1.5).
 \end{aligned} \tag{A14}$$

**Data pre-processing** In order to train the priors, we transformed the coordiantes into the ENU system and normalized them. ENU coordinates, short for East-North-Up coordinates, are a type of Cartesian coordinate system commonly used in geodesy, navigation, and earth sciences to represent positions on or near the Earth’s surface. The ENU coordinate system is a local, tangential coordinate system that is centered at a specific reference point on the Earth’s surface.

**Neural network training details.** Data for neural network training were drawn from the uniform prior on the lengthscale. The neural network was trained for  $n_{\text{epochs}} = 10000$  epochs, with  $n_{\text{batch}} = 2000$  batch size, and  $1e^{-3}$  learning rate. Value of the  $\sigma_{\text{vae}}^2$  hyperparameter was set to 0.8.

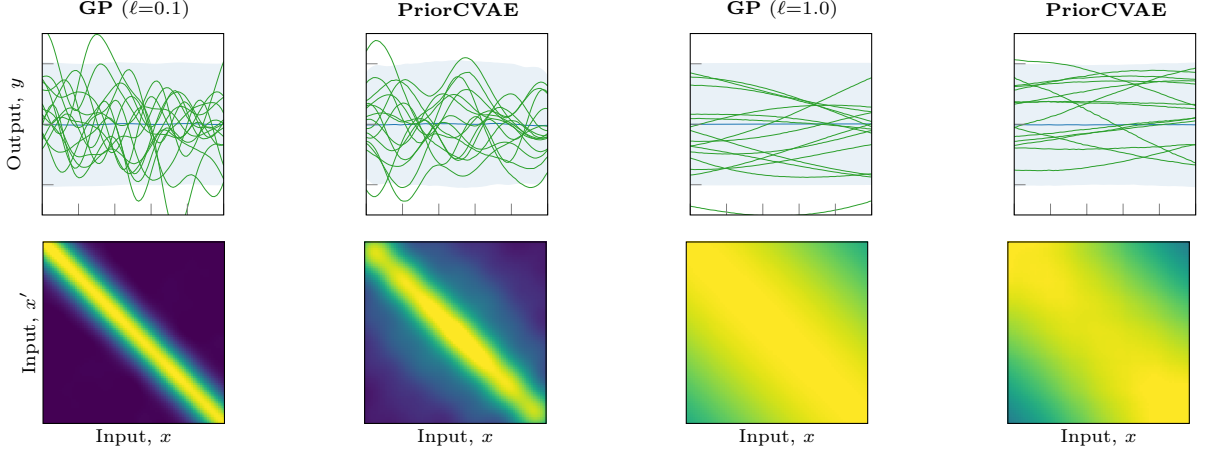


Figure A10: **Our PriorCVAE samples and covariance resemble the original GP.** Example draws (top) and computed Gram (covariance) matrices (bottom, 0 1) from a Squared Exponential (RBF) prior with lengthscale  $\ell = 0.1$  (two left-hand columns) and  $\ell = 1.0$  (two right-hand columns).

**Comparison with R-INLA.** R-INLA (Lindgren and Rue, 2015) is a popular software for Bayesian spatial modelling and is viewed as state-of-the-art in many applied fields. While being very fast, R-INLA has limitations, such as, for example, it does not permit RBF kernel, or Matérn kernels with smoothness higher than  $\nu = \alpha - m/2$ , where  $\alpha \in (0, 2]$  and  $m$  is space dimensionality. In our case,  $m = 2$ , hence, the highest available smoothness is  $\nu = 1$ . In order to compare hyperparameter estimates, we need to align R-INLA parameterisation with Matérn kernel parameterisation that we use. Denote the distance between a pair of points as  $\|s\| = \|c_i - c_j\|$ . Then our parameterisation is

$$C_\nu(\|s\|) = \sigma^2 \frac{2^{1-\nu}}{\Gamma(\nu)} \left( \sqrt{2\nu} \frac{\|s\|}{l} \right)^\nu K_\nu \left( \sqrt{2\nu} \frac{\|s\|}{l} \right), \quad (\text{A15})$$

and R-INLA parameterisation is

$$C_\nu(\|s\|) = \sigma^2 \frac{2^{1-\nu}}{\Gamma(\nu)} (\kappa \|s\|)^\nu K_\nu(\kappa \|s\|), \quad (\text{A16})$$

$$\sigma^2 = \frac{\Gamma(\nu)}{\Gamma(\alpha)(4\pi)^{m/2} \kappa^{2\nu} \tau^2}. \quad (\text{A17})$$

Priors in R-INLA are provided with respect to parameters

$$\theta_1 = \log(\tau), \quad (\text{A18})$$

$$\theta_2 = \log(\kappa). \quad (\text{A19})$$

Hence, lengthscale can be recovered from R-INLA parameterisation as

$$l = \frac{\sqrt{2\nu}}{\kappa} = \frac{\sqrt{2\nu}}{\exp(\theta_2)}, \quad (\text{A20})$$

and for  $m = 2, \nu = 1, \alpha = 2$  we get (since  $\Gamma(1) = \Gamma(2) = 1$ )

$$\sigma^2 = \frac{1}{4\pi \kappa^2 \tau^2} = \frac{1}{4\pi \exp^2(\theta_2) \exp^2(\theta_1)}. \quad (\text{A21})$$

While we attempted a head-to-head comparison, R-INLA's interface for setting priors was not flexible enough to easily allow this. Hence we conducted a sensitivity analysis, which showed that the R-INLA posteriors were not sensitive to the prior choice. Comparison of parameter estimates produced by PriorCVAE and R-INLA are shown on Fig. A9. However, they should be taken with caution since, as explained, they use the same kernel (Matérn- $5/2$ ), the priors used by the two models were different.

## F SIR: Training Details

In this experiment, the values of  $(\beta, \gamma)$  act as a conditional vector for the PriorCVAE model, which is defined with the hidden dimensions as 10, latent dimension as 6 and leaky-ReLU activation function. We train the PriorCVAE model for 10000 iterations with 2000 batch size and Adam optimizer with  $10^{-3}$  learning rate. We put a uniform prior on both the  $\beta$  and the  $\gamma$  parameter,  $\mathcal{U}(0, 1)$ . The data for training was scaled by  $N$ , so that the values of the learnt curve  $I(t)$  were scaled to the  $(0, 1)$  range:  $I(t)/N$ .

## G Double-Well

We experiment to encode the non-linear Double-Well diffusion process (DP) using the PriorCVAE model. The Double-Well DP is defined by an SDE

$$dx_t = \theta_1 x_t (\theta_2 - x_t^2) + d\beta_t \tag{A22}$$

with  $\theta_1, \theta_2$  being the parameters of the DP, and  $Q$  is the spectral density.

We simulate trajectories from the DP with two sets of parameters  $(\theta_0=2; \theta_1=3)$ , and  $(\theta_0=4; \theta_1=1)$  using Euler-Maruyama for  $T = [0, 20]$  with  $\Delta t = 0.01$ . The values of  $\theta = (\theta_0, \theta_1)$  act as a conditional vector for the PriorCVAE model, which is defined with the hidden dimensions as  $[1000, 500, 100]$ , latent dimension as 50 and sigmoid activation function. We train the PriorCVAE model for 5000 iterations with 2000 batch size and Adam optimizer with  $10^{-3}$  learning rate.

Fig. A7 shows the learnt samples from PriorCVAE along with the samples from the true Double-Well DP. The plot also shows the histogram of states which clearly shows two wells depending on the  $\theta$  values.

## H Software, and Reproducibility

We provide a sample code as a proof-of-concept with this supplementary. In terms of the implementation, the neural network models were implemented with JAX (Bradbury et al., 2018) in Python. Bayesian inference, including NUTS, Laplace approximation and ADVI, were implemented in NumPyro (Phan et al., 2019; Bingham et al., 2019) using JAX as the backend.

## I Probabilistic Programming Example with NumPyro

```

1 # PriorCVAE decoder as a function of neural network parameters expressed
2 # in terms of 'jax.numpy' (jnp) tensors
3 def c_decoder_numpy(z, W1, B1, W2, B2, c):
4
5     def linear(z, W, B):
6         lin_out = jnp.matmul(z, W) + B
7         return lin_out
8         c = jnp.array(c).reshape(1)
9         z = jnp.concatenate([z, c], axis=0)
10
11     hidden = jax.nn.relu(linear(z, W1, B1))
12     out = linear(hidden, W2, B2)
13     return out
14
15 # Numpyro model for inference
16 def numpyro_model(z_dim, conditional=False, y=None, obs_idx=None):
17
18     # priors
19     c = numpyro.sample("c", npdist.Uniform(0.01, 0.99))
20     z = numpyro.sample("z", npdist.Normal(jnp.zeros(z_dim), jnp.ones(z_dim)))
21     sigma = numpyro.sample("sigma", npdist.HalfNormal(0.1))
22
23     # deterministic transformation
24     f = numpyro.deterministic("f", c_decoder_numpy(z, W1, B1, W2, B2, c))
25

```



```
26     # likelihood
27     y = numpyro.sample("y", npdist.Normal(f[obs_idx], sigma), obs=y)
28
29 # Setup and run MCMC
30 kernel = NUTS(numpyro_model)
31 mcmc = MCMC(kernel,
32             num_warmup=args["num_warmup"], # number of warmup steps
33             num_samples=args["num_samples"], # number of posterior steps
34             num_chains=args["num_chains"] # number of chains
35 )
```

Listing 1: Probabilistic programming example

## J Supplementary Figures.

This section contains supplementary figures of the experiments.

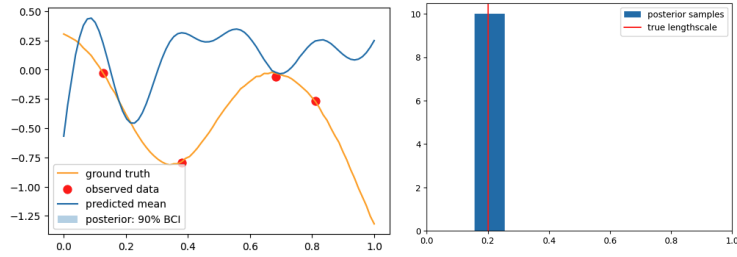


Figure A11: Laplace approximation inference results produced by Google Colab: left - mean and uncertainty, right - hyperparameter estimate.

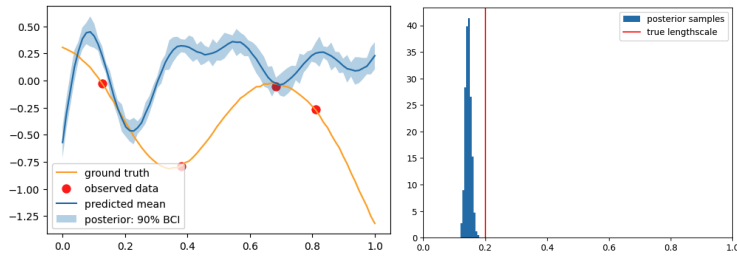


Figure A12: ADVI inference results produced by Google Colab: left - mean and uncertainty, right - hyperparameter estimate.

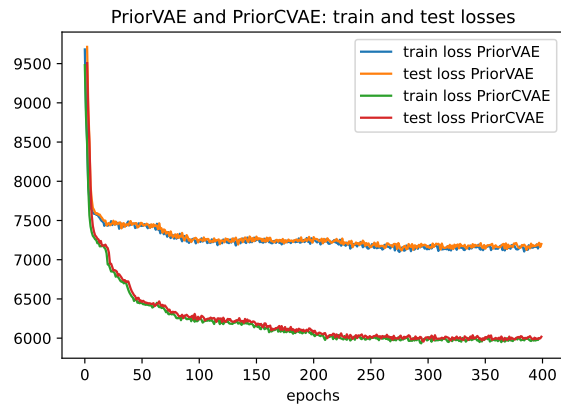


Figure A13: Training and test losses of PriorVAE and PriorCVAE models.

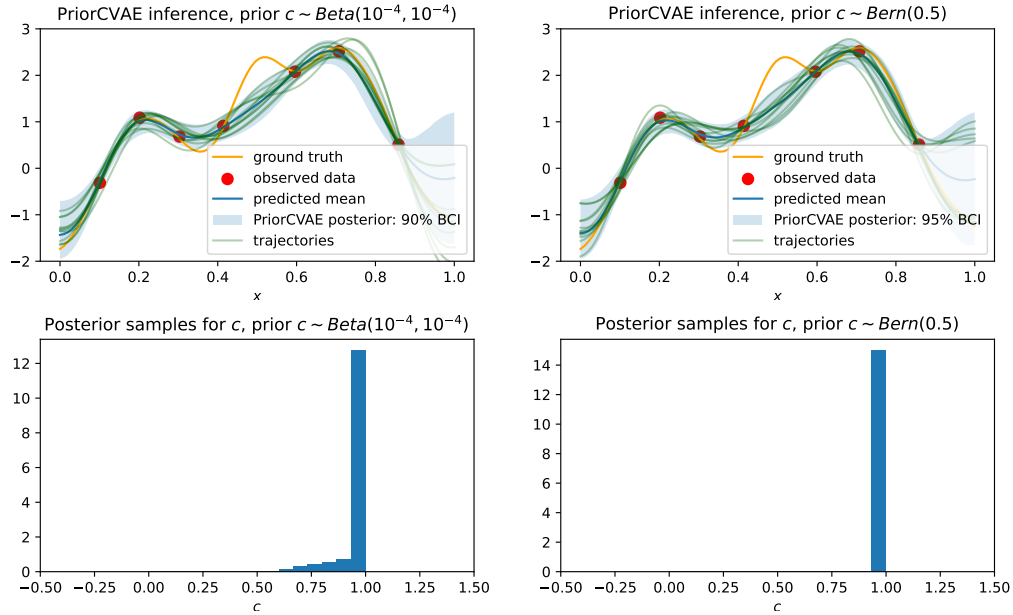


Figure A14: Left: inference performed using NUTS and PriorCVAE with a binary condition, approximating the true Bernoulli prior with a continuous Beta prior. Right: inference performed using MixedHMC and PriorCVAE with a binary condition, inferred as a discrete variable with a Bernoulli prior.

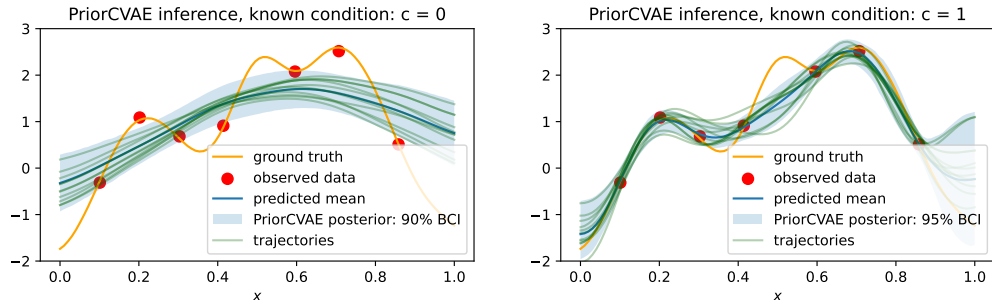


Figure A15: Inference performed using NUTS and PriorCVAE, assuming the binary condition  $c$  is known. Left:  $c = 0$  (misspecified model), right:  $c = 1$  (correctly specified model).

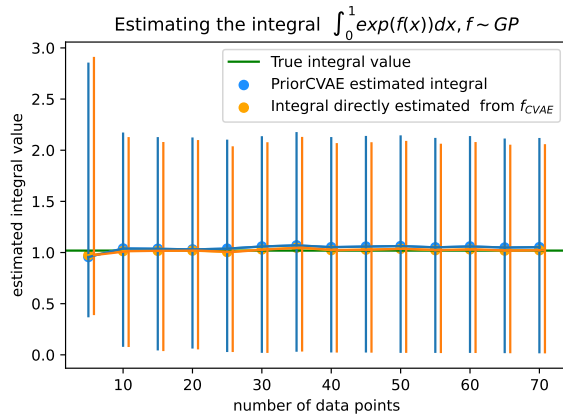


Figure A16: Encoding  $\int_0^1 \exp(f(x))dx$ . The graph shows the mean estimate and uncertainty over five runs of the two methods to compute the integral: the first method uses encoded integral values directly, and the second uses  $f_{\text{PriorCVAE}}$  draws and then computes the integral.

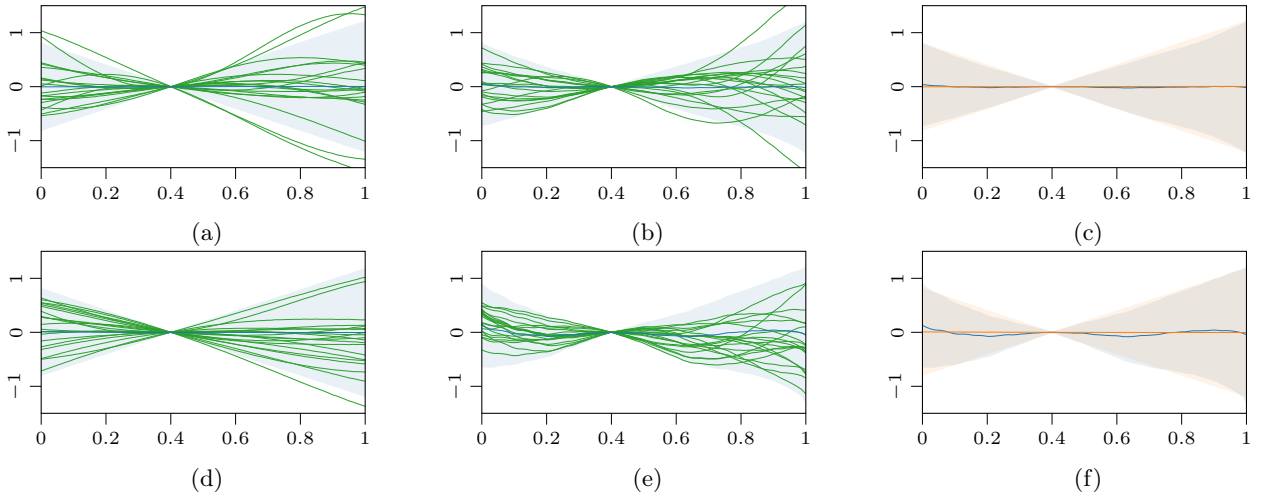


Figure A17: **Non-stationary kernel:** (a) Priors drawn from a GP kernel ( $\ell = 0.5$ ) . (b) Learnt priors from the PriorCVAE model ( $\ell = 0.5$ ) . (c) Comparison of the second moments of the GP and PriorCVAE model ( $\ell = 0.5$ ). (d) Priors drawn from a GP kernel ( $\ell = 0.9$ ). (e) Learnt priors from the PriorCVAE model ( $\ell = 0.9$ ). (f) Comparison of the second moments of the GP and PriorCVAE model ( $\ell = 0.9$ ).

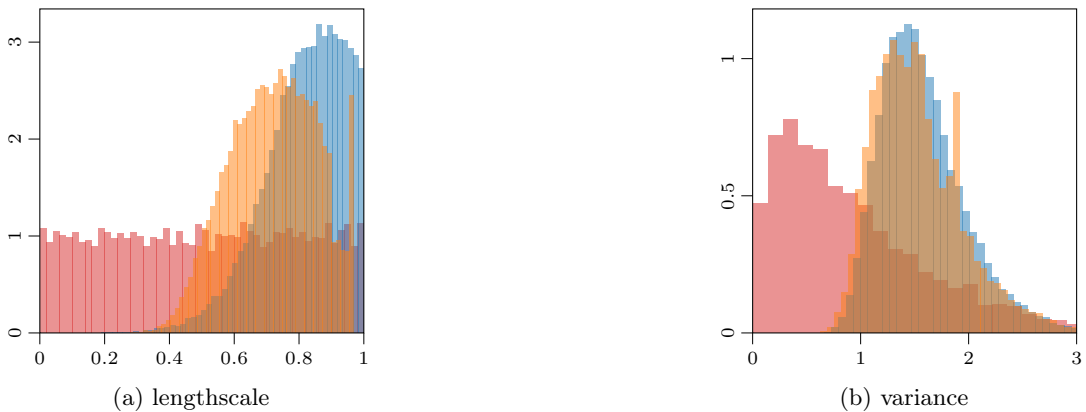


Figure A18: Parameter estimates produced by models with  $f_{\text{GP}}$  and  $f_{\text{PriorCVAE}}$  priors.



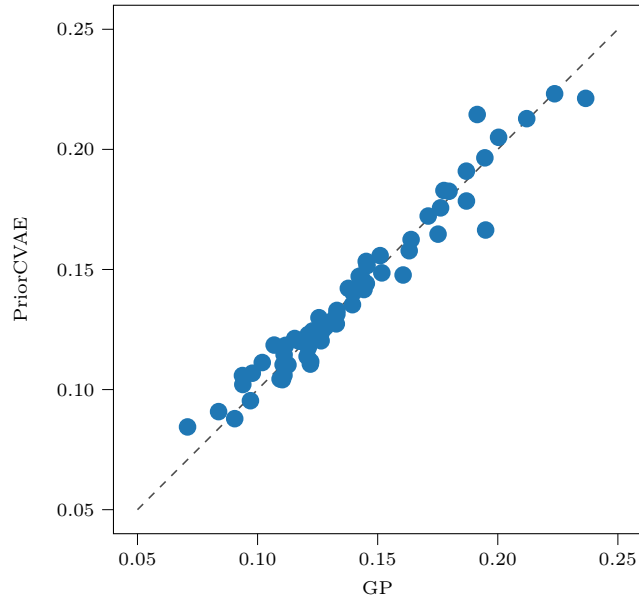


Figure A19: Comparison of estimated prevalence of HIV in Zimbabwe obtained using the original  $f_{GP}$  prior, and the model with the  $f_{PriorCVAE}$  prior.

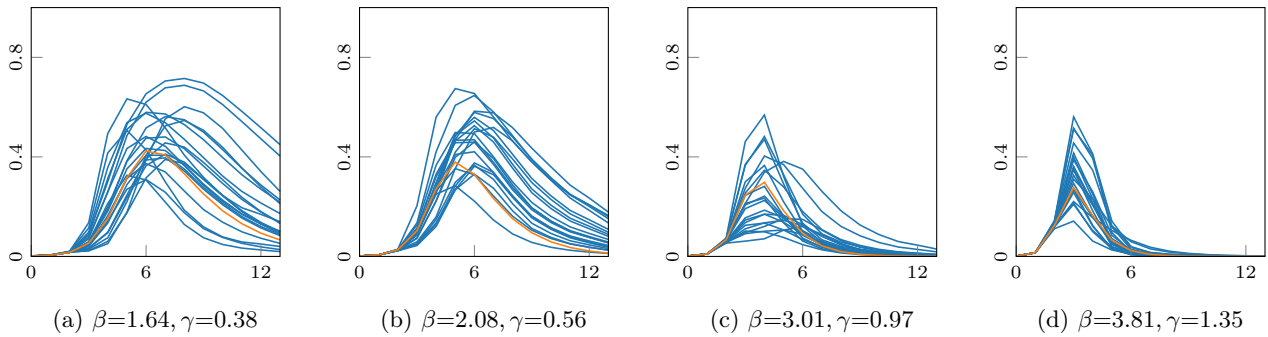


Figure A20: **SIR experiment:** Prior samples — from the trained PriorCVAE model for different values of  $\beta$  and  $\gamma$  along with the ODE solution —. The ODE solution is always enveloped by the PriorCVAE samples.

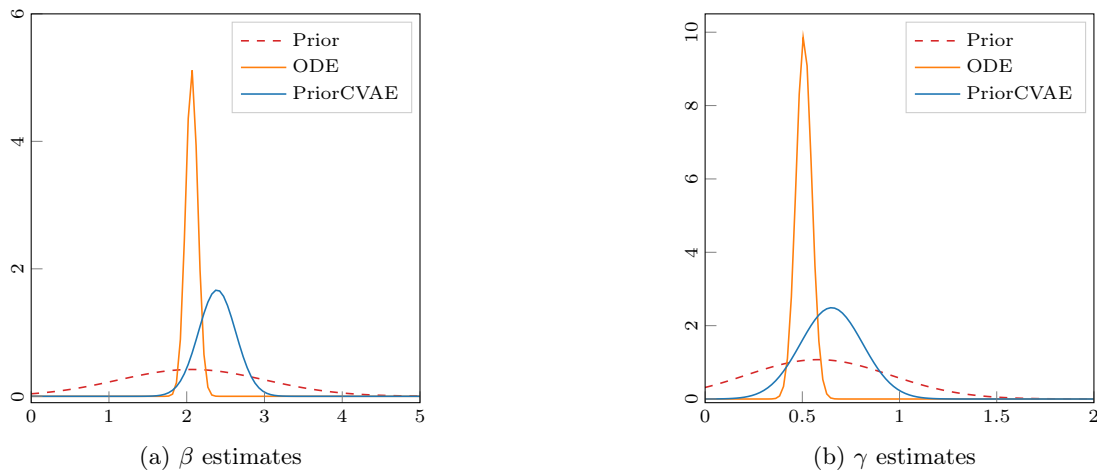


Figure A21: **SIR experiment:** MCMC parameter estimates of the ODE and the PriorCVAE model.